TITLE: Comparison of two excilamps and two reactor configurations in the UV-H_2O_2 removal process of amaranth.

Authors: M.D. Murcia, M. Gómez, E. Gómez, J.L. Gomez*, A.M. Hidalgo, S. Murcia, D. Campos

Chemical Engineering Department. University of Murcia. Spain.

*Corresponding author. Email: carrasco@um.es. Phone: +34 868887351. Fax: +34 868884148.

Keywords: Amaranth; UV photodegradation; excilamps; flow-through photoreactor; kinetic model.

Abstract

Nowadays dyes are used in many industrial activities and their presence in wastewater is quite common and involves different environmental and health problems. In addition, dyes are usually recalcitrant compounds and conventional treatment are not appropriate for their removal. So there is great interest in finding alternative removal processes, as the one based on excimer lamp technology for the removal of amaranth dye described in the present work. Two excilamps and two reactor configurations have been tested: a batch reactor with KrCl or XeBr excilamp and a KrCl flow-through photoreactor. After comparing the results for both lamps in the batch reactor, the KrCl excilamp has proven to be more efficient both in terms of conversions achieved and energy consumption and, by this, it has been selected to be used in the flow-through photoreactor. For both reactor configurations, several experimental series were done to analyze the influence of the different operational variables on the photoprocess and the optimal mass ratio between hydrogen peroxide and dye has been established. Also, it has been proven that the use of Fenton reagent improves the process efficiency, particularly in the case of the XeBr lamp.

In addition, a kinetic model, based on a previous one developed by the authors for a flow-through photoreactor and slightly modified to can also apply it to batch reactors, has been applied. The model has been validated with an excellent fitting of the experimental data for all series and both reactor configurations.

1. INTRODUCTION

With the aim to increase sales, companies tend to offer more attractive products, something that can be achieved by means of color, since it allows us to differentiate the products, makes them more striking or customize them. Industries such as cosmetics, food or textile are just some examples of this tendency. Dyes can also be used for more technical purposes, such as those found in pharmacy or laboratories.

The main problem derived from the multiple applications of dyes is the presence of colored compounds in wastewater that will end up being discharged into the natural environment. Despite the apparently innocuous aesthetic effects on the receptor medium, the transmission of solar energy decreases by the presence of dyes and this affects the photosynthesis and reduces the concentration of oxygen in the ecosystem. In addition, some of these compounds may be toxic to organisms of the aquatic medium [1, 2], affecting their development or behaviour [3, 4]. Another important aspect of dyes is that, in some cases, the products formed during their decomposition can become more toxic than the dyes themselves.

Azo dyes are the most common and numerous dyes and among them amaranth has been the one selected for this research. It is used in the coloration of textile fibers, leather, paper, thermoplastics, wood, cosmetics, inks and in the food industry with the number E123 of the International Numbering System (INS) [5]. Amaranth also has applications in biological research, such as detecting changes in membranes potential [5]. According to some recent research studies, as one with in vitro human lymphocytes [6], it seems that amaranth can be toxic and, by this, it is not authorized anymore in EEUU as additive in the food, pharmaceutical and cosmetic industry. As a consequence, amaranth can be considered as a pollutant which must be removed from wastewaters.

Different physical, chemical and biological methods have been used for the removal of amaranth from wastewaters. Adsorption treatments have been tested with good results with adsorbent materials such as zeolites or activated carbon [7]. However this technique involves the pollutant change of phase and by this, although almost total removal from wastewater can be achieved, the pollutant remains in the adsorbent, which must be treated further. Membrane processes have been applied as well among the physical treatments, using nanofiltration and reverse osmosis with polysulfone and polyethylamine membranes [8, 9]. In this case the main disadvantage is the high energy consumption and also the concentrate obtained that must be treated as well. Biological treatments have been used with bacterial culture such as *Pseudomonas* [10], fungi [11] or peroxidase enzymes extracted from *Arundo donax*, *Typha angustifolia* or *Phragmites australis* [12], however, due to the toxicity of pollutants, some of these treatments can be applied only for low dye concentrations.

Chemical methods like coagulation-flocculation, ionic exchange or electro-coagulation have proven to be effective for the removal of azo dyes like amaranth [13, 14, 15]. Among the chemical methods, oxidation processes offer the important advantage that total mineralization of the pollutant can be achieved in most cases. Subcritical and supercritical water oxidation have been used attaining removal efficiencies of azo dyes between 80-90% [16, 17], although extreme temperature and pressure conditions are normally required for these treatments.

Advanced oxidation processes (AOPs) offer an interesting alternative that has been attracting increasing interest over the last years. AOPs are based on the generation of strong oxidizing agents, like HO•, allowing oxidation and total mineralization of water pollutants even at very low concentrations due to their high reactivity and low selectivity [18]. Both photochemical and non-photochemical AOPs such as ozonation

[19], Fenton treatment [20] or UV-Fenton [21] have been successfully used for amaranth removal from wastewater.

Among the photochemical AOPs, excimer technology has been selected for the present work because in the literature there are no references about the use of this technology in the removal of this dye. Excimer lamps or excilamps are new UV sources based on transitions of exciplex (rare gas halides) or excimer molecules (rare gas or halogen dimmers) formed as a result of an electric discharge. They are attractive alternatives to commonly used mercury lamps because they have some important advantages including the absence of elemental mercury, long lifetime (from 1000 to 10000 h), geometric freedom and high photon flux. Their main advantage is the emission in a narrow-band UV radiation, nearly monochromatic and matching the dissociation energies of bonds of the main organic compounds, especially if barrier discharge lamps are used since they provide a narrower emission spectrum. From an environmental point of view, the absence of toxic mercury is a remarkable characteristic [22-25]. Over the last years excimer technology has been applied to the removal of different organic pollutants that can be found in industrial wastewaters, using different lamp configurations [26-37].

In addition, different kinetic studies on oxidation treatments of amaranth and other dyes can be found in the literature [38-41]. In most processes the progress curves can be successfully fitted to a pseudo first order kinetic model and, commonly, the first order kinetic parameter shows a dependence on the operational variables, mainly the concentration of pollutant, which is not the expected behaviour for a true first order kinetics. In a previous work [42] the authors studied the photodegradation of the methylene blue dye using an exciplex KrCl flow-through photoreactor, and a kinetic model, that explained the dependence of the first order kinetic parameter on the operational variables, was developed and successfully validated.

In the present paper, a comparative study is carried out, firstly in a batch reactor with two different excilamps of KrCl and XeBr, to test their efficiency in the removal of amaranth. Once the best lamp is selected, the second part of the study is focused on the photodegradation of amaranth by using an exciplex KrCl flow-through photoreactor. This is the reactor configuration that allows us to work, in the future, not only in discontinuous but also in semicontinuous or continuous mode, as a previous step for a further scale-up of the process. In addition, the previously developed kinetic model, with some small modifications to be suitable for batch reactors, is checked and validated with the data obtained from both reaction systems.

2. MATERIALS AND METHODS

2.1. Reagents

Amaranth (85-95% w/w) was purchased from Sigma-Aldrich Fine Chemicals, hydrogen peroxide (33% w/v) was purchased from Panreac, ferrous sulphate was purchased from Probus, catalase solution (1340 U/mg solid) and aluminium potassium sulphate (≥ 98,0%) were purchased from Sigma-Aldrich Fine Chemicals. Other chemicals were of analytical grade and were used without further purification.

2.2. Materials

The equipment used for the experiments consist in two barrier discharge excilamps (purchased from the Institute of High Current Electronics of the Siberian Branch, Russian Academy of Sciences). The XeBr and KrCl excilamps emitting maximum UV radiation at 283 and 222 nm, respectively, were of cylindrical geometry covered by a metal case having an UV exit window with an area of 75 cm^2. The exit window was oriented at a fixed distance of 3 cm over a vessel of 100 mL of capacity and 4.5 cm

external diameter. The average radiation intensity delivered to the solution was 17.12 and 2.47 $mWcm^{-2}$ for XeBr and KrCl excimer lamps, respectively.

Also a flow-through KrCl photoreactor with an irradiation zone length of 30 cm and an internal diameter of 2 cm, which provides an irradiation area of 188.5 cm^2 and with an average radiation intensity of 2.38 $mWcm^{-2}$ was used in the experiments.

Data of radiation intensity, both for the two excilamps and for the flow-through photoreactor, were provided by the manufacturer.

For the analytical determination of amaranth concentration, an ultraviolet/visible Thermospectronic Helios Alpha spectrophotometer was used. COD was also measured with some specific equipment consisting of reactor and photometer, model HI 938800 and model 83099, respectively, from HANNA Instruments. An eppendorf centrifuge 5424 was used in Fenton's series.

2.3. Operational procedure

Photodegradation assays were done in two configurations of reactors: a batch reactor with KrCl and XeBr excilamp and a KrCl flow-through photoreactor.

In the first case a glass beaker is used as a batch reactor, excilamp is over the reactor and radiation directly falls on the treated volume. A system scheme is presented in Figure 1A. Amaranth, hydrogen peroxide and Fe^{2+}, at the required concentrations, were dissolved in distilled water and placed into the glass beaker and irradiated at room temperature (23–25 ºC), under static conditions and for exposure times of 120 min. For the different experiments, fluence was also determined by multiplying the radiation intensity and the exposure time of reaction volume.

In the second case, the solution containing the amaranth and the rest of the reagents (hydrogen peroxide and Fe^{2+}), at the required initial concentration, was pumped from a stirred tank to the photoreactor and the effluent was continuously recycled to the tank, so that the system acts as a pseudo-batch reactor (flow-through reactor). All the experiments were done at room temperature (23–25 ºC), with an operational time of 120 min. Experimental equipment, including the main components, is depicted in Figure 1B.

In both cases, samples were taken at different reaction times (0, 2.5, 5, 10, 20, 40, 60, 90 and 120 min). Duplicate experiments were carried out and average values were obtained.

Four experimental series were carried out, in order to study the influence of the following operational variables: H_2O_2:amaranth mass ratio, initial amaranth concentration, reaction volume and initial Fe^{2+} concentration. Experimental conditions, for all the experiments with the static excilamps and for the KrCl flow-through photoreactor, are shown in Tables 1 and 2.

2.4. Analytical determinations

Samples were spectrophotometrically analyzed at the amaranth maximum absorption wavelength in the visible region (522 nm). Absorbance values were transformed to concentrations by using the amaranth calibration curve: [Amaranth] (mg/L) = $Absorbance_{522}$ / 0.0399 (r = 0.9998).

3. KINETIC MODEL

The kinetic model applied in the present work is an adaptation of another one previously developed [42], with small modifications to be suitable for batch reactors. The model is based on the presence of two regions with different dye concentration in

the liquid phase: a thin layer in the region where the radiation is delivered to the solution, where the photoprocess takes place, with a small residual concentration of non degraded dye, and the bulk solution, with a uniform concentration of dye, which decreases with time and is the measured concentration. The model takes into account the dependence of the first order kinetic constant on different experimental variables, a behaviour that does not correspond to a true first order kinetic, but to a pseudo-first order one. The model has been applied to the data from both the KrCl photoreactor and the batch reactor with KrCl and XeBr excilamps, being the equations valid for both systems. In the following, the model hypotheses and equations are presented.

3.1. Model hypotheses

I. Both the stirring in the glass beaker and the flow rate in the photoreactor are high enough and, as a consequence, the solution is well agitated and the amaranth concentration in the bulk solution, $[A]$, only varies with time.

II. Different consecutive steps take place along the photodegradation process of amaranth, from the initial dye to intermediate compounds until the final products. The global reaction can be expressed as:

$$Amaranth + n\,H_2O_2 \rightarrow Intermediates \rightarrow Final\ products \qquad (equation\ 3.1)$$

III. At any time, if $[A]_0$ and $[A]$ are the initial and current mass concentrations of the dye, respectively, and $[Prod]_i$ is the mass concentration of each one of the products formed, according to the mass conservation law it must be verified:

$$[A] + \sum [Prod]_i = [A]_0 \qquad (equation\ 3.2)$$

IV. The radiation intensity delivered to the sample from the KrCl photoreactor or from the KrCl and XeBr excilamps is constant at a fixed distance from the UV

source and uniformly distributed. So a density of radiation intensity per mass unit can be expressed as the quotient $I/[A]_0$, where I is the average radiation intensity emitted.

V. The radiation is quickly absorbed by the substrates and photoproducts and consumed during the photoprocess near the region where it is delivered to the solution. So it can be assumed that the photodegradation takes place in a thin film, with a small volume V_R, close to the top of the reactor volume, for the batch experiments with KrCl and XeBr, and close to the wall of the quartz tube in the KrCl photoreactor. As a result there are two regions with different dye concentrations: the thin film where the photoprocess takes place, with a small residual concentration $[A]_{lim}$, and the bulk solution, whose volume V is practically equal to the sample volume, with a uniform concentration $[A]$ which decreases with time, according to hypothesis I. These two regions determines a transport of amaranth which will be a limiting step, being the driven force the concentration gradient $[A] - [A]_{lim}$.

VI. In a similar way as explained in the above hypothesis for amaranth, there is a concentration gradient of hydrogen peroxide, $[H_2O_2]$-$[H_2O_2]_{lim}$. However this mass transfer is faster than the one of amaranth and not limiting due to the much lower molecular weight of hydrogen peroxide.

VII. The photodegradation of amaranth takes place both by direct photolysis and by reaction with hydrogen peroxide.

3.2. Model equations

As previously indicated, in the assays with KrCl and XeBr excilamps a glass beaker was used as a batch reactor, and in the experiments carried out with the photoreactor, total recirculation was used, so the system acts as a batch reactor as well. As a result, for both

reactor configurations, if r_A is the amaranth photodegradation rate, V the total sample volume and V_R the volume of the reaction zone, the mass balance can be expressed as follows:

$$V\frac{d[A]}{dt} + V_R r_A = 0 \qquad (equation\ 3.3)$$

According to hypothesis V, and being $k_L a$ the mass transfer volumetric coefficient, the mass transfer rate, r_{dif}, can be expressed as:

$$r_{dif} = k_L a([A] - [A]_{\text{lim}}) \qquad (equation\ 3.4)$$

Taking into account hypothesis IV, the energy received in the time unit by the mass of amaranth must be proportional to the mass transfer rate and to the density of radiation per mass unit, being k_E the proportionality constant:

$$E_A = k_E k_L a\frac{I}{[A]_0}([A] - [A]_{\text{lim}}) \qquad (equation\ 3.5)$$

And taking into account the quantum yield of the process, the photodegradation rate can be defined as follows:

$$r_A = \varepsilon k_E k_L a\frac{I}{[A]_0}([A] - [A]_{\text{lim}}) \qquad (equation\ 3.6)$$

According to hypothesis VII, and if k_{c1} is the kinetic constant of direct photolysis and k_{c2} is the kinetic constant of the photodegradation with hydrogen peroxide, the following equation applies:

$$r_A = k_{C1}[A]_{lim} + k_{C2}[A]_{lim}[H_2O_2]_{\text{lim}} \qquad (equation\ 3.7)$$

From these last two equations (3.6) and (3.7) the value of $[A]_{lim}$ can be obtained:

$$[A]_{\text{lim}} = \frac{\varepsilon k_E k_L a I[A]}{\varepsilon k_E k_L a I + k_{C1}[A]_0 + k_{C2}[H_2O_2]_{\text{lim}}\,[A]_0} \qquad (equation\ 3.8)$$

And by replacing this expression in equation (3.7) a new equation for r_A is obtained:

$$r_A = \frac{\varepsilon k_E k_L a I\left(k_{C1} + k_{C2}[H_2O_2]_{lim}\right)}{\varepsilon k_E k_L a I + \left(k_{C1} + k_{C2}[H_2O_2]_{lim}\right)[A]_0}[A] \qquad (equation\ 3.9)$$

By substituting equation (3.9) in equation (3.3) of mass balance, the variation of [A] with time can be obtained as follows:

$$\frac{d[A]}{dt} = -\frac{V_R \quad \varepsilon k_E k_L a I \left(k_{C1} + k_{C2}[H_2O_2]_{lim}\right)}{V\ \varepsilon k_E k_L a I + \left(k_{C1} + k_{C2}[H_2O_2]_{lim}\right)[A]_0}[A] \qquad (equation\ 3.10)$$

From Eq. (3.10), a pseudo-first order kinetic constant, k_r, can be defined as:

$$k_r = \frac{V_R \quad \varepsilon k_E k_L a I \left(k_{C1} + k_{C2}[H_2O_2]_{lim}\right)}{V\ \varepsilon k_E k_L a I + \left(k_{C1} + k_{C2}[H_2O_2]_{lim}\right)[A]_0} \qquad (equation\ 3.11)$$

And since $[H_2O_2]_{lim}$ has a small value, the approximation $k_{C1} + k_{C2}[H_2O_2]_{lim} = k_{C1}$ can be accepted and it leads to a new expression for the pseudo-first order kinetic constant, k_r:

$$k_r = \frac{V_R \quad k_{C1} \varepsilon k_E k_L a I}{V\ \varepsilon k_E k_L a I + k_{C1}[A]_0} \qquad (equation\ 3.12)$$

The definition of k_r allows us to simplify the mass balance equation to the following one, matching the batch reactor equation for a pseudo-first order kinetic:

$$\frac{d[A]}{dt} = -k_r[A] \qquad (equation\ 3.13)$$

Additionally, from the definition of conversion:

$$X_A = \frac{[A]_0 - [A]}{[A]_0} \qquad (equation\ 3.14)$$

Equation (3.13) is modified to:

$$\frac{dX_A}{dt} = k_r(1 - X_A) \qquad (equation\ 3.15)$$

With the initial condition:

$t = 0; \quad X_A = 0 \qquad (equation\ 3.16)$

Finally, from the integration of equation (3.15), it is obtained:

$$X_A = 1 - e^{-k_r \cdot t} \qquad (equation\ 3.17)$$

For the fitting of the experimental data to equation (3.17), the software Curve Expert 1.4 has been used.

4. RESULTS AND DISCUSSION

As indicated at the end of section 2.3, four experimental series were carried out, in order to study the influence of the different operational variables on the process. In Figure 1 the experimental reaction system is shown, and the experimental conditions for the four series are shown on Table 1, for the KrCl and XeBr static excilamps, and on Table 2, for the KrCl flow-through photoreactor.

Regarding the results, the ones obtained for the four experimental series, both for the KrCl And XeBr static excilamps, are presented in Figures 2 to 6 and discussed in subsections 4.1 and 4.2. In a similar way, the ones for the flow-through photoreactor can be found in Figures 7 to 8 and they are discussed in subsections 4.3 and 4.4. Finally, in subsection 4.5, a comparison between the results obtained in this work and some others found in similar studies, has been made.

4.1. Experimental results in batch reactor with KrCl and XeBr excilamps

In the first experimental series the influence of the variation of H_2O_2:amaranth mass ratio on the process has been analyzed. The results obtained are shown in Figures 2A and 2B for the KrCl and XeBr excilamp, respectively. As it can be observed, for the KrCl lamp the optimum mass ratio seems to be 5:1, and there is no significant improvement with the results corresponding to the 6:1 ratio. In a similar way, for the XeBr lamp the optimal ratio seems to be 6:1.

Once the optimum mass ratio has been selected for both lamps the obtained results were compared, not only considering the photodegradation rate but also the energy consumption expressed as fluence. This can be seen in Figures 2C and 2D, proving that the KrCl excilamp is clearly more effective, both in terms of degradation rate and energy consumption. This result can be explained taking into account the wavelength of

maximum UV emission of both excilamps, which is 222 nm for the KrCl excilamp, very close to the maximum absorption wavelength of amaranth in the UV region (225 nm), while this maximum is of 283 nm for the XeBr excilamp, far from amaranth absorption.

It is important to notice that, although the average radiation intensity of the XeBr lamp is around 5 times higher than the one of the KrCl excilamp, the most determining factor to achieve an optimum photodegradation process is the matching between the maximum emission of the lamp and the maximum absorption of the target compound. This aspect is particularly relevant when monochromatic sources, such as excimer lamps, are used.

In Figure 3A, which corresponds with the second series and where the variation of the initial dye concentration was studied, it can be seen that, for both excilamps, conversion decreases when increasing amaranth initial concentration, as expected, since the radiation intensity per mass unit is lower. As in the previous series, the best results are obtained with the KrCl lamp, also considering the energy consumption, as it can be seen in Figure 3B.

The third experimental series, in which reaction volume was varied, is depicted in Figures 4A and 4B, showing the variation of conversion versus time and fluence, respectively. From these results it seems that this variable has no significant influence, probably due to the narrow range of volume variation used in this series. Once again, the KrCl has proven to be the best UV source, achieving high values of amaranth conversion with low energy requirements.

Finally, for the four series, the results corresponding to the Photo-Fenton process are shown in Figures 5A to 5D. It is interesting to observe how the use of Fenton improves the performance of the XeBr excilamp. For the optimum Fe^{2+} concentration selected,

5 mg/L, the results of the mentioned lamp are very close to the ones obtained with the KrCl excilamp, which is still a better option, especially in terms of fluence.

4.2. Model fitting of the batch reactor results with KrCl and XeBr excilamps

In Figures 2 to 5, the dots are the experimental values of conversion and the continuous lines correspond with the data calculated by using equation (3.17). Additionally, in Table 1 the values of the pseudo first order kinetic constant, k_r , obtained in the fitting of the experimental data of each series to the model, and the correlation coefficients are shown. As it can be observed, both in all Figures and in Table 1, an excellent fitting to the proposed model has been obtained.

In the series with the variation of the H_2O_2:amaranth mass ratio, to analyze the dependence of k_r on the experimental conditions equation (3.11) must be applied, since the only variable is the hydrogen peroxide concentration. However, as the value of $[H_2O_2]_{Lim}$ is unknown, some approximation must be made. Assuming this value is almost proportional to the initial hydrogen peroxide concentration, being k_H the proportionality constant, the rate constant obtained from equation (3.11) can be rewritten as:

$$k_r = \frac{V_R \quad \varepsilon k_E k_L a I (k_{C1} + k_{C2} k_H [H_2O_2]_0)}{V \, \varepsilon k_E k_L a I + (k_{C1} + k_{C2} k_H [H_2O_2]_0)[A]_0} \qquad (equation\ 4.1)$$

And by putting all constants together, the following dependence with $[H_2O_2]_0$ is obtained:

$$k_r = \frac{a + b[H_2O_2]_0}{c + d[H_2O_2]_0} \qquad (equation\ 4.2)$$

Figure 6A shows the fitting to this previous equation using the different values of $[H_2O_2]_0$ and the calculated values of k_r for both KrCl and XeBr excilamps. The values

of the different parameters of equation (4.2) are presented in Table 3, where the high correlation coefficients obtained are also shown. In Figure 6A it is also important to point out the much higher values of k_r obtained for the KrCl excilamp, in good agreement with the better performance of this UV lamp mentioned in section 4.1.

For the fitting to the model of experimental series 2, where the variation of initial dye concentration was studied, from equation (3.12) the following new expression can be obtained:

$$\frac{1}{k_r} = \frac{V}{V_R} \cdot \left(\frac{1}{\varepsilon k_E k_L a I} [A]_0 + \frac{1}{k_{C1}} \right) \qquad (equation\ 4.3)$$

Which can be expressed as follows:

$$\frac{1}{k_r} = a'[A]_0 + b' \qquad (equation\ 4.4)$$

The good fitting to this last equation is shown in Figure 6B. And once again, the values of k_r are higher for the assays with the KrCl excimer lamp, as expected from the experimental results.

In the third series, equation (3.12) has been used again for the model fitting. A linear variation of k_r with the inverse of the volume is expected initially according to the following expression:

$$k_r = \frac{1}{V} \left(\frac{V_R (k_{C1} \varepsilon k_E k_L a I)}{\varepsilon k_E k_L a I + k_{C1} [A]_0} \right) \qquad (equation\ 4.5)$$

However, as it can be seen in Figure 6C, there is not a significant variation of k_r with the inverse of V, as predicted in equation (4.5). This is probably due to a double and opposite effect. On one hand, as the volume is in the denominator of equation (4.5), a higher volume has a negative effect on the kinetic constant. On the other hand, taking

into account the experimental system used, a higher volume involves less distance between the free surface of reaction volume and the radiation source and, as a result, the sample receives higher radiation intensity and the value of k_r increases. As a consequence of this double effect and considering, also, the narrow range obtained for the variation of k_r, there is no clear tendency for this series.

Finally, for the Photo-Fenton experiments, although the use of Fenton reagent is not considered in the model equations, the same kinetic model has been applied with good results, and a clear linear dependence between the obtained values of k_r and the variation of the initial Fe^{2+} concentration is presented in Figure 6D, being again the KrCl excilamp more efficient.

4.3. Experimental results in the KrCl flow-through photoreactor

Results from this experimental reactor configuration are shown in Figure 7. Figure 7A depicts the results of variation in the H_2O_2:amaranth mass ratio. As it can be observed, the optimum mass ratio seems to be 2.5:1.0, because for a higher mass ratio (3.0:1.0) no significant improvements are obtained. After selecting the optimum mass ratio, the influences of variation of the initial dye concentration and the reaction volume were studied. Results are depicted in Figures 7B and 7C, respectively, showing that conversion decreases when there is an increase in amaranth initial concentration and/or in the reaction volume, in good agreement with the behaviour predicted in equations (4.4) and (4.5). This is the expected result, as the radiation intensity is the same but lower per mass unit.
Finally, Figure 7D shows the results corresponding to the Photo-Fenton process, where it can be noticed that, even with the lowest Fe^{2+} concentration assayed, the reaction is very fast and conversion values close to 100% are reached from the first reaction minutes.

4.4. Model fitting of the KrCl flow-through photoreactor results

As indicated in previous paragraphs, in Figure 7 solid lines correspond with the fitting to the model of the experimental data, for each experimental series. Also, the values of k_r and correlation coefficients can be found in Table 2. Figures 7A to 7C show an excellent fitting of the experimental data to the model.

Figure 8A shows the fitting to equation (4.2) for the different values of k_r obtained in the series of variation of H_2O_2:amaranth mass ratio. Table 4 shows the values of the different parameters of equation (4.2), as well as the high correlation coefficient obtained. In the same way, Figure 8B shows the fitting of k_r to equation (4.4) for the experimental data corresponding to the variation of the initial dye concentration. A good fitting is observed and, also, a decreasing in k_r values for increasing values of initial dye concentration, as expected.

For the third series, and taken into account that in this reactor configuration there is no variation in the intensity of radiation, since the distance from the radiation source and the liquid surface is constant, according to equation (4.5) a linear variation of k_r with the inverse of the volume is expected. Figure 8C shows the obtained fitting.

Finally, for the Photo-Fenton experiments, as it has been previously commented, the use of Fenton reagent is not considered in the model equations. Besides, the reaction occurs very fast and the progress curve is practically a constant line, as shown in Figure 7D.

4.5. Comparison with other similar studies.

Regarding the amaranth degradation rate, it must be taken into account that it depends on the different operational conditions: The dye concentration, the type of UV lamp used, the use of an oxidizing agent and the possible addition of a catalyst. As a

consequence it is not easy to make a comparison between the results obtained in this work and the ones from other published manuscripts on similar studies.

Nevertheless, a comparison has been made using the results of the present study and the ones obtained by Gomathi et al., [21], and Wu et al., [40]. These works have been selected because their results have been fitted to a pseudo-first order kinetic model as well, and the values of the pseudo-first order kinetic constant can be found, which facilitates the comparison.

In this way, from equation (3.17) of the manuscript, where the relationship between the conversion, X_A, the reaction time, t, and the kinetic constant, k_r, was established, the half-life time, $t_{1/2}$, can be calculated as follows:

$$t_{1/2} = -\frac{Ln(0.5)}{k_r} \qquad (equation\ 4.6)$$

This time corresponds with a conversion of 0.5, and it is the time needed to degrade half of the initial dye concentration. So, the lower the half-life time is the higher is the efficiency of the lamp. Also, if the intensity of radiation is known, the fluence corresponding to the half-life time can be also calculated, and the lower the fluence, the lower the energy consumption.

From these considerations, in Table 5, a comparison between the results obtained for the half-life time and fluence in this work and the ones calculated from the data shown in references [21] and [40] has been made. As it can be seen in Table 5, in terms of half-life time and fluence the higher efficiency corresponds with the KrCl excilamp, being the efficiency of the XeBr excilamp higher or lower than the one of reference [21], depending on the initial dye concentration, and lower than the one of reference [40].

So, it can be affirmed that good removal performance of amaranth can be obtained with excilamps, mainly with the KrCl one. Additionally, as the use of mercury is avoided in these lamps, they are also a technology cleanest and more environmentally friendly than traditional UV sources.

5. CONCLUSIONS

Excimer technology has proven to be an excellent alternative to conventional treatments for the removal of complex organic compounds such as dyes, achieving a high elimination level under optimal reaction conditions. In this work, two reactor configurations have been used for the photodegradation of amaranth: a batch reactor with KrCl or XeBr excilamp and a KrCl flow-through photoreactor.

Firstly, a detailed study comparing the results attained with the KrCl and XeBr excilamps in the discontinuous system has been carried out. The KrCl lamp has led to the best results, both in terms of removal efficiency, amount of oxidant needed (optimum mass ratio hydrogen peroxide: dye is 5:1 versus 6:1 for the XeBr) and energy requirements, although with the addition of Fenton reagent as oxidant there is a significant improvement in the results obtained with the XeBr excilamp, being very close to those achieved with the KrCl lamp.

Once the KrCl excilamp has been selected, the flow-through photoreactor has been tested for the same experimental series. For this reactor configuration, the optimal mass ratio hydrogen peroxide:amaranth has been 2.5:1 and, as previously, the photo-Fenton process significantly improves the removal efficiencies.

In addition, a kinetic model, previously developed by the authors and slightly modified to be suitable for batch reactors, has been tested and validated with an excellent fitting

of all experimental data for both reactor configurations. This model agrees with the observed dependence of the pseudo-first order kinetic constant on different experimental variables.

Future research must be focused on the process scale-up and, for that, semicontinuous or continuous configurations of the flow-through photoreactor must be tested and some small aspects of the kinetic model must be improved, such as the inclusion of the Fenton reagent in the model equations or a deeper study of the influence of the reaction volume distance from the radiation source, allowing an even better process simulation and understanding.

6. ACKNOWLEDGEMENTS

Along this work, M.D. Murcia was beneficiary of "Ramon y Cajal" contract (2016) from MINECORYC-2016-20211

7. NOMENCLATURE

A	Amaranth
a	Parameter defined in Eq. 4.2, (mg L^{-1} min^{-2})
a'	Parameter defined in Eq. 4.4, (mg^{-1} L min)
b	Parameter defined in Eq. 4.2, (mg L^{-1} min^{-2})
b'	Parameter defined in Eq. 4.4, (min)
c	Parameter defined in Eq. 4.2, (mg L^{-1} min^{-1})
d	Parameter defined in Eq. 4.2, (mg L^{-1} min^{-1})
E_A	Energy received in the time unit by amaranth, (W min^{-1})

ε	Quantum yield defined in Eq. 3.6, (mg L^{-1} W^{-1})
I	Intensity of radiation, (W)
k_{c1}	Kinetic constant of direct photolysis in the film, (min^{-1})
k_{c2}	Kinetic constant with hydrogen peroxide in the film, ($mg^{-1}L^{-1}min^{-1}$)
k_E	Proportionallity constant defined in Eq. 3.5, (dimensionless)
k_La	Volumetric mass transfer coefficient, (min^{-1})
k_r	Pseudo first order kinetic constant, (min^{-1})
r	Correlation coefficient, (dimensionless)
r_A	Reaction rate, (mg $L^{-1}min^{-1}$)
r_{dif}	Mass transfer rate, (mg $L^{-1}min^{-1}$)
t	Reaction time, (min)
$t_{1/2}$	Half-life reaction time, (min)
V	Volume of bulk solution, (mL)
V_R	Volume of photoreaction zone in the film, (mL)
X_A	Conversion of amaranth, (dimensionless)
$[A]$	Concentration of amaranth at time t, (mg L^{-1})
$[A]_0$	Initial concentration of amaranth, (mg L^{-1})
$[A]_{Lim}$	Concentration of amaranth in the film, (mg L^{-1})
$[H_2O_2]$	Concentration of hydrogen peroxide at time t, (mg L^{-1})

$[H_2O_2]_0$ Initial concentration of hydrogen peroxide, (mg L^{-1})

$[H_2O_2]_{Lim}$ Concentration of hydrogen peroxide in the film, (mg L^{-1})

$[Prod]_i$ Concentration of product i, (mg L^{-1})

8. REFERENCES

[1] S. Kobylewski, M.F. Jacobson, Toxicology of food dyes, Int. J. Occup. Environ. Health 18(3) (2012) 220-246. https://doi.org/10.1179/1077352512Z.00000000034

[2] A. Bafana, S.S. Devi, T. Chakrabarti, Azo dyes: past, present and the future, Environ. Rev. 19(1) (2011) 350-370. https://doi.org/10.1139/a11-018

[3] F.R. Abe, A.M.V.M Soares, D.P.D. Oliveira, C. Gravato, Toxicity of dyes to zebra fish at the biochemical level: Cellular energy allocation and neurotoxicity, Environ. Pollut. 235 (2018) 255-262. https://doi.org/10.1016/j.envpol.2017.12.020

[4] P. Soni, S. Sharma, S. Sharma, S. Kumar, K.P. Sharma, A comparative study on the toxic effects of textile dye wastewaters (untreated and treated) on mortality and RBC of a freshwater fish Gambusiaaffinis (Baird and Gerard), J. Environ. Biol. 27(4) (2006) 623-628.

[5] R.W. Sabnis, Handbook of Biological Dyes and Stains: Synthesisand Industrial Applications, John Wiley&Sons, Inc., Hoboken, New Jersey, 2010. DOI:10.1002/9780470586242

[6] A. Basu, G.S. Kumar, Interaction of toxic azo dyes with heme protein: Biophysical insights into the binding aspect of the food additive amaranth with human hemoglobin, J. Hazard. Mater. 289 (2015) 204-209. http://dx.doi.org/10.1016/j.jhazmat.2015.02.044

[7] K.Y. A. Lin, C.H. Wu, Efficient adsorptive removal of toxic amaranth dye from water using a zeolitic imidazolate framework, Water Environ. Res. 90(11) (2018) 1947-1955. https://doi.org/10.2175/106143017X14902968254692

[8] J.R. Hollahan, T. Wydeven, Synthesis of Reverse-Osmosis Membrane by

Plasma Polymerization of Allylamine, Science, 179 (1973) 500-501. DOI:10.1126/science.179.4072.500

[9] M. Min, L. Shen, G. Hong, M. Zhu, Y. Zhang, X. Wang, Y. Chen, B.S. Hsiao, Micro-nano structure poly(ether sulfones)/poly(ethyleneimine) nanofibrous affinity membranes for adsorption of anionic dyes and heavy metal ions in aqueous solution, Chem. Eng. J. 197 (2012) 88-100. https://doi.org/10.1016/j.cej.2012.05.021

[10] M. Belouhova, I. Schneider, S. Chakarov, I. Ivanova, Y. Topalova, Microbial community development of biofilm in amaranth decolourization technology analysed by FISH, Biotechnol. Biotechnol. Equip. 28 (2014) 635-642. https://doi.org/10.1080/13102818.2014.947725

[11] C. Rani, A.K. Jana, A. Bansal, Potential of different white rot fungi to decolourize textile azo dyes in the absence of external carbon source, Environ. Technol. 33 (2012) 887-896. https://doi.org/10.1080/09593330.2011.602431

[12] D. Haddaji, L. Bousselmi, O. Saadani, I. Nouairi, Z. Ghrabi-Gammar, Enzymatic degradation of azo dyes using three macrophyte species: *Arundo donax*, *Typha angustifolia* and *Phragmites australis*, Desalin. Water Treat. 53 (2015) 1129-1138. https://doi.org/10.1080/19443994.2014.884475

[13] V. Golob, A. Vinder, M. Simonič, Efficiency of the coagulation/flocculation method for the treatment of dye bath effluents, Dyes pigm. 67(2) (2005) 93- 97. https://doi.org/10.1016/j.dyepig.2004.11.003

[14] A. Szyguła, E. Guibal, M. A. Palacín, M. Ruiz, A.M. Sastre, Removal of an anionic dye (Acid Blue 92) by coagulation-flocculation using chitosan, J. Environ. Manage. 90(10) (2009) 2979-2986. https://doi.org/10.1016/j.jenvman.2009.04.002

[15] S. Raghu, C. Ahmed, Chemical or electrochemical techniques, followed by ion exchange, for recycle of textile dye wastewater, J. Hazard. Mater. 149(2) (2007) 324-330. https://doi.org/10.1016/j.jhazmat.2007.03.087

[16] B. Kayan, B. Gözmen, Degradation of Acid Red 274 using H_2O_2 in subcritical water: Application of response surface methodology, J. Hazard. Mater. 201-202 (2012) 100-106. https://doi.org/10.1016/j.jhazmat.2011.11.045

[17] Z. Chen, Z. Chen, F. Ying, G. Wang, H. Chen, C. He, Y. Xu, Supercritical water oxidation of oil-based drill cuttings, J. Hazard. Mater. 332 (2017) 205-213. https://doi.org/10.1016/j.jhazmat.2017.03.001

[18] R. Andreozzi, V. Caprio, A. Insola, R. Marotta, Advanced oxidation processes (AOP) for water purification and recovery, Catal. Today. 53(1) (1999) 51-59. https://doi.org/10.1016/S0920-5861(99)00102-9

[19] C.Z.A. Abidin, M.R. Fahmi, O. Soon-An, S.N.N.M. Makhtar, N.R. Rahmat, Decolourization of an azo dye in aqueous solution by ozonation in a semi-batch bubble column reactor, Scienceasia 41(1) (2015) 49-54. doi: 10.2306/scienceasia1513-1874.2015.41.049

[20] W.R.P. Barros, P.C. Franco, J.R. Steter, R.S. Rocha, M.R.V. Lanza, Electro-Fenton degradation of the food dye amaranth using a gas diffusion electrode modified with cobalt (II) phthalocyanine, J. Electroanal. Chem. 722-723 (2014) 46-53. https://doi.org/10.1016/j.jelechem.2014.03.027

[21] L. Gomathi, K. Eraiah, K.S. Anantha, S. Girish, Influence of various aromatic derivatives on the advanced photo Fenton degradation of Amaranth dye, Desalination 270(1-3) (2011) 31-39. https://doi.org/10.1016/j.desal.2010.11.017

[22] U. Kogelschatz, Excimer lamps: History, discharge physics, and industrial applications, P. Soc. Photo-Opt. Inst. 5483 (2004) 272-286.

https://doi.org/10.1117/12.563006

[23] T. Oppenländer, Photochemical Treatment of Water: Comparison of Incoherent Excimer Lamps with a Medium-Pressure Mercuy Lamp, Chem. Eng. Technol. 21(6) (1998) 502-505.

https://doi.org/10.1002/(SICI)1521-4125(199806)21:6<502::AID-CEAT502>3.0.CO;2-0

[24] M.I. Lomaev, E.A. Sosnin, V.F. Tarasenko, D.V. Shits, V.S. Shakun, M.V. Erofeev, A.A. Lisenko, Capacitive and Barrier Discharge excilamps and their applications (Review), Instrum. Exp. Tech. 49(5) (2006) 595-616.
DOI:10.1134/S0020441206050010

[25] V.F. Tarasenko, E.A. Sosnin, O.S. Zhdanova, E.P. Krasnozhenov, Applications of excilamps in microbiological and medical investigations.In: Z. Machala, K. Hensel, Y. Akishev (eds) Plasma for Bio-Decontamination, Medicine and Food Security. NATO Science for Peace and Security Series A: Chemistry and Biology. Springer, Dordrecht (2012) 251-263.

https://doi.org/10.1007/978-94-007-2852-3_19

[26] E.A. Sosnin, T. Oppenländer, V.F. Tarasenko, Applications of capacitive and barrier discharge excilamps in photoscience, J. Photochem. Photobiol. C-Photochem. Rev. 7(4) (2006) 145-163.

https://doi.org/10.1016/j.jphotochemrev.2006.12.002

[27] G. Matafonova, N. Christofi, V. Batoev, E. Sosnin, Degradation of

chlorophenols in aqueous media using UV XeBr excilamp in a flow-through reactor, Chemosphere 70(6) (2008) 1124-1127.

https://doi.org/10.1016/j.chemosphere.2007.08.022

[28] V. B. Batoev, G. G. Matafonova, and N. I. Filippova,Direct Photolysis of Chlorophenols in Aqueous Solutions by UV Radiation from Excilamps, Russian Journal of Applied Chemistry, 84 (2011) 407–411.

DOI:10.1134/S1070427211030128

[29] M. Gómez, M.D. Murcia, E. Gómez, J.L. Gómez, N. Christofi, Degradation of phenolic pollutants using KrCl and XeBr excilamps in the presence of dye: A comparative study, Desalination 274(1-3) (2011) 156-163.

https://doi.org/10.1016/j.desal.2011.02.004

[30] A.C.V. Dos Santos, J.C. Masini, Development of a flow through photo-reactor to study degradation of organic compounds by sequential injection analysis (SIA), J. Braz. Chem. Soc. 20(10) (2009) 1800-1804.

http://dx.doi.org/10.1590/S0103-50532009001000005

[31] I. Tsenter**,** G. Matafonova, V. Batoev, Combination of high-frequency ultrasound and UV radiation of excilamp for surface disinfection, Eng. Life Sci. 15 (2015) 830–834. DOI:10.1002/elsc.201500073

[32] G. Matafonova, V. Batoev,Recent advances in application of UV light-emitting diodes for degrading organic pollutants in water through advanced oxidation processes: A review, Water Research 132 (2018) 177-189.

https://doi.org/10.1016/j.watres.2017.12.089

[33] M. Gomez, M.D. Murcia, N. Christofi, E. Gomez, J.L. Gomez, Photodegradation of 4-chlorophenol using XeBr, KrCl and Cl_2 barrier-discharge excilamps: A comparative study, Chem. Eng. J. 158(2) (2010) 120-128.

https://doi.org/10.1016/j.cej.2009.12.015

[34] G. Matafonova, V. Batoev, Comparison of energy requirements for removal of organic micropollutants from lake water and wastewater effluents by direct UV and UV/H2O2 using excilamp, Desalination and Water Treatment, 85 (2019) 92-102. DOI: 10.5004/dwt.2017.21245

[35] M. Gomez, M.D. Murcia, J.L. Gomez, E. Gomez, M.F. Maximo, A. García, A KrCl exciplex flow-through photoreactor for degrading 4-chlorophenol: Experimental and modelling, Appl. Catal. B-Environ. 117-118 (2012) 194-203.

https://doi.org/10.1016/j.apcatb.2012.01.017

[36] S. Popova, G. Matafonova, V. Batoev, Simultaneous atrazine degradation and E. coli inactivation by UV/$S_2O_8^{2-}$/Fe^{2+} process under KrCl excilamp (222 nm) irradiation, Ecotoxicology and Environmental Safety 169 (2019) 169–177.

https://doi.org/10.1016/j.ecoenv.2018.11.014

[37] M.D. Murcia, M. Gómez, E. Gómez, J.L. Gómez, N. Christofi, Photodegradation of congo red using XeBr, KrCl and Cl_2 barrier discharge excilamps: A kinetics study, Desalination 281(1) (2011) 364-371.

https://doi.org/10.1016/j.desal.2011.08.011

[38] Q. Zhang, C. Li, T. Li, Rapid photocatalytic decolorization of methylene blue using high photon flux UV/TiO_2/H_2O_2 process, Chem. Eng. J. 217 (2013) 407-413. https://doi.org/10.1016/j.cej.2012.11.106

[39] P. Dachipally, S.B. Jonnalagadda, Kinetics of ozone-initiated oxidation of textile dye, Amaranth in aqueous systems, J. Environ. Sci. Health Part A-Toxic/Hazard. Subst. Environ. Eng. 46(8) (2011) 887-897.

https://doi.org/10.1080/10934529.2011.580201

[40] C.H. Wu, C.L. Chang, C.Y. Kuo, Decolorization of Amaranth by advanced oxidation processes, React. Kinet. Catal. Lett. 86(1) (2005) 37-43.

https://doi.org/10.1007/s11144-005-0292-4

[41] V.K. Gupta, R. Jain, A. Mittal, T.A. Saleh, A. Nayak, S. Agarwal, S. Sikarwar, Photo-catalytic degradation of toxic dye amaranth on TiO_2/UV in aqueous suspension, Mater. Sci. Eng. C 32(1) (2012) 12-17.

https://doi.org/10.1016/j.msec.2011.08.018

[42] M. Gómez, M.D. Murcia, E. Gómez, S. Ortega, A. Sánchez, O. Thaikovskaya, N. Briantceva, Modelling and experimental checking of the influence of substrate concentration on the first order kinetic constant in photo-processes, J. Environ. Manage. 183 (2016) 818-825.

https://doi.org/10.1016/j.jenvman.2016.09.033

Figure 1

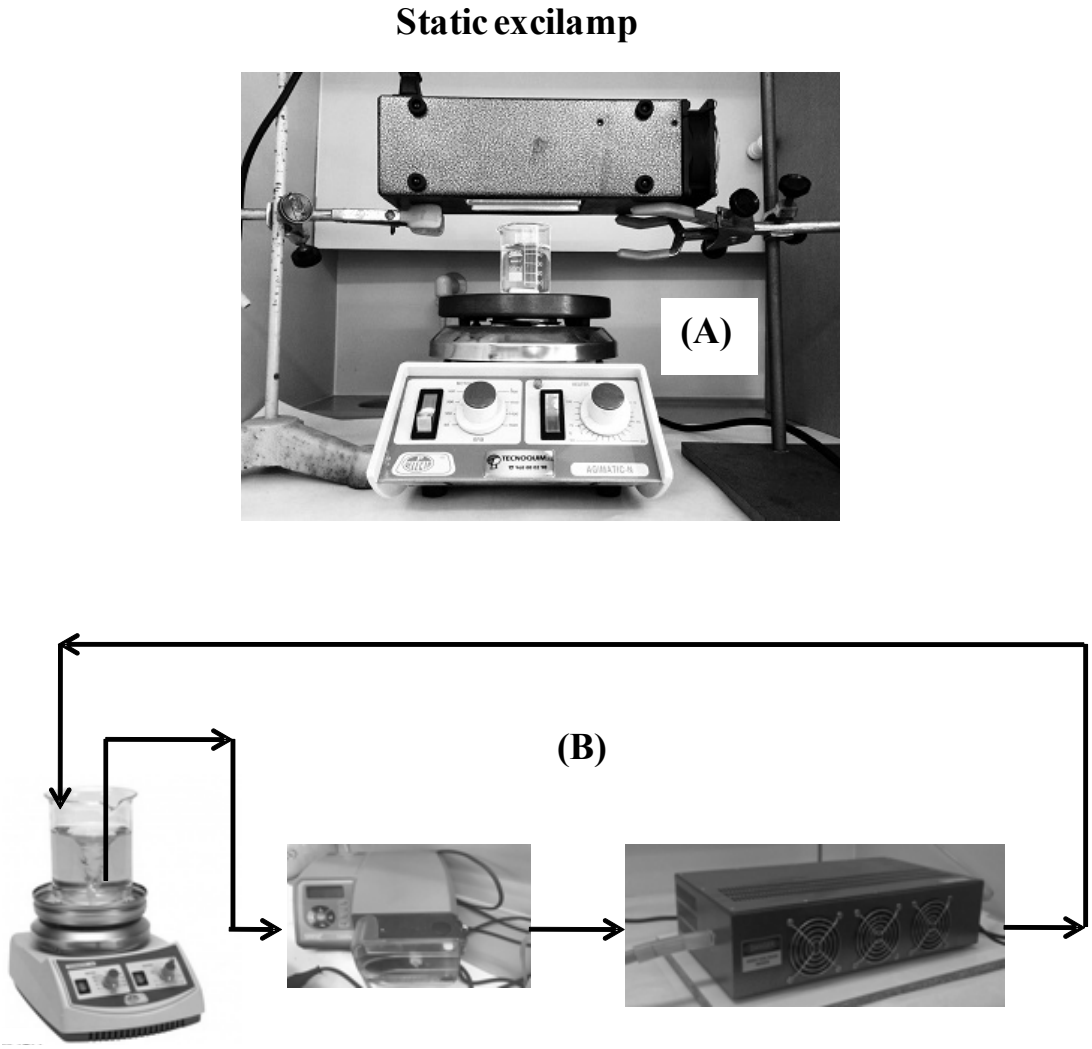

Figure 1. Experimental reaction system, **(A)**: Static excilamp batch reactor and **(B)**:KrCl flow-through photoreactor.

Figure 2

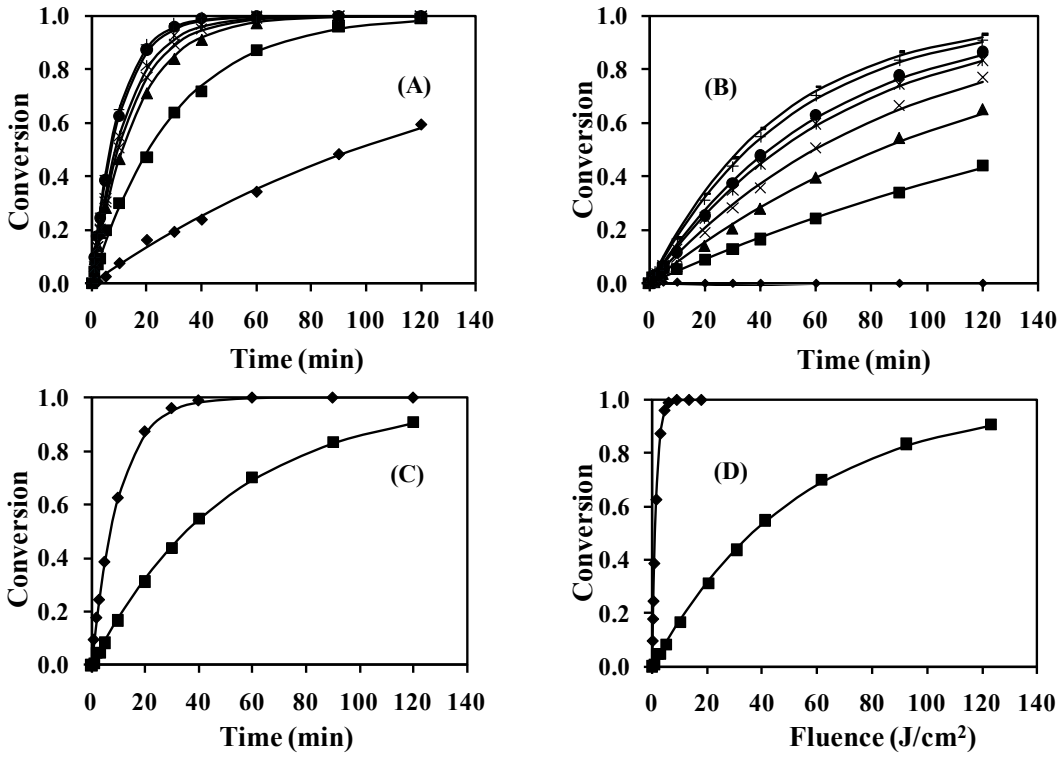

Figure 2. Variation of $[H_2O_2]_0$:$[A]_0$ mass ratio; Amaranth conversion versus time, experimental and calculated values. **(A)**: KrCl excilamp. $[A]_0$ = 100 mg L^{-1}, V = 50 mL, $[Fe^{2+}]_0$ = 0 mg L^{-1}, $[H_2O_2]_0$:$[A]_0$ mass ratio = ♦ 0:1, ■1:1, ▲2:1, x 3:1, *4:1, ●5:1, + 6:1, (-) model. **(B)**: XeBr excilamp. $[A]_0$ = 100 mg/l, V = 50 mL, $[Fe^{2+}]_0$ = 0 mg L^{-1},mass ratio $[H_2O_2]_0$:$[A]_0$ = ♦ 0:1, ■1:1, ▲2:1, x 3:1, *4:1, ●5:1, + 6:1, - 7:1, (-) model. **(C)**: Amaranth conversion versus time for the optimum $[H_2O_2]_0$:$[A]_0$ mass ratio. Excilamp: ♦KrCl, ■ XeBr, (-) model. **(D)**: Amaranth conversion versus fluence for the optimum $[H_2O_2]_0$:$[A]_0$ mass ratio. Excilamp: ♦KrCl, ■ XeBr, (-) model.

Figure 3

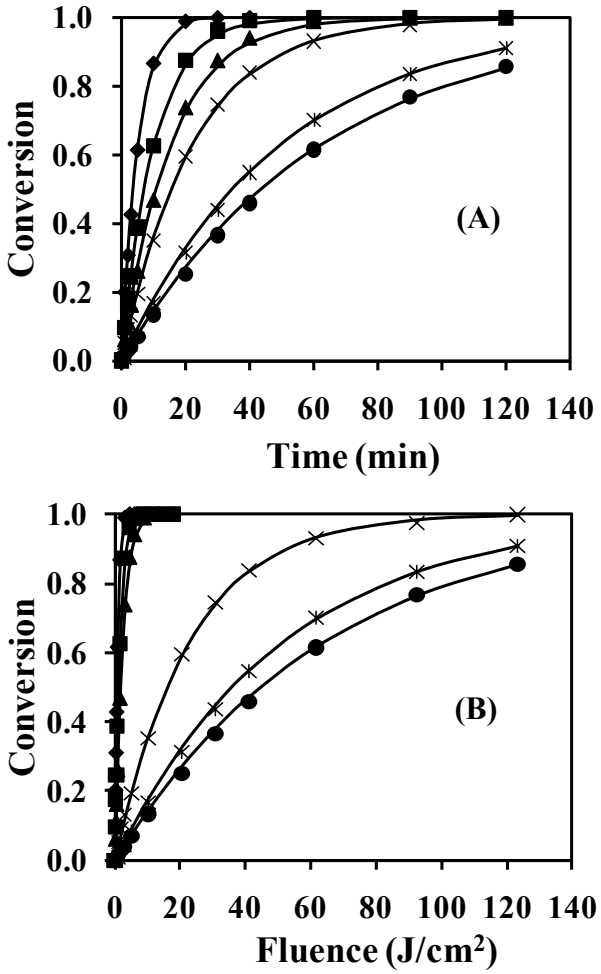

Figure 3. Variation of amaranth initial concentration, **(A)**: Amaranth conversion versus time, experimental and calculated values. **(B)**: Amaranth conversion versus fluence. Mass ratio $[H_2O_2]_0$:$[A]_0$ = 5:1 for KrCl and 6:1 for XeBr, V = 50 mL, $[Fe^{2+}]_0$ = 0 mg L^{-1}. Variation of $[A]_0$ (mg L^{-1}) = ♦KrCl 50, ■ KrCl 100, ▲KrCl 150, xXeBr 50, *XeBr 100, ●XeBr 150, (-) model.

Figure 4

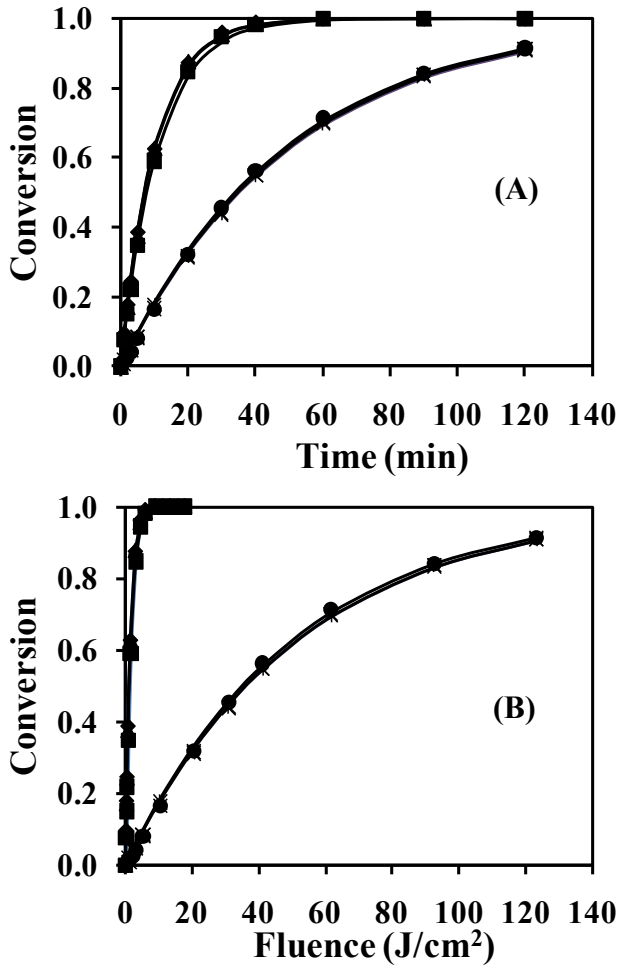

Figure 4. Variation of reaction volume **(A)**: Amaranth conversion versus time, experimental and calculated values. **(B)**: Amaranth conversion versus fluence. $[A]_0$ = 100 mg L^{-1}, mass ratio $[H_2O_2]_0$:$[A]_0$ = 5:1 for KrCl and 6:1 for XeBr, $[Fe^{2+}]_0$ = 0 mg L^{-1}. Variation of V (mL) = ♦KrCl 50, ■KrCl 70, ▲KrCl 90, xXeBr 50, *XeBr 70, ●XeBr 90, (-) model.

Figure 5

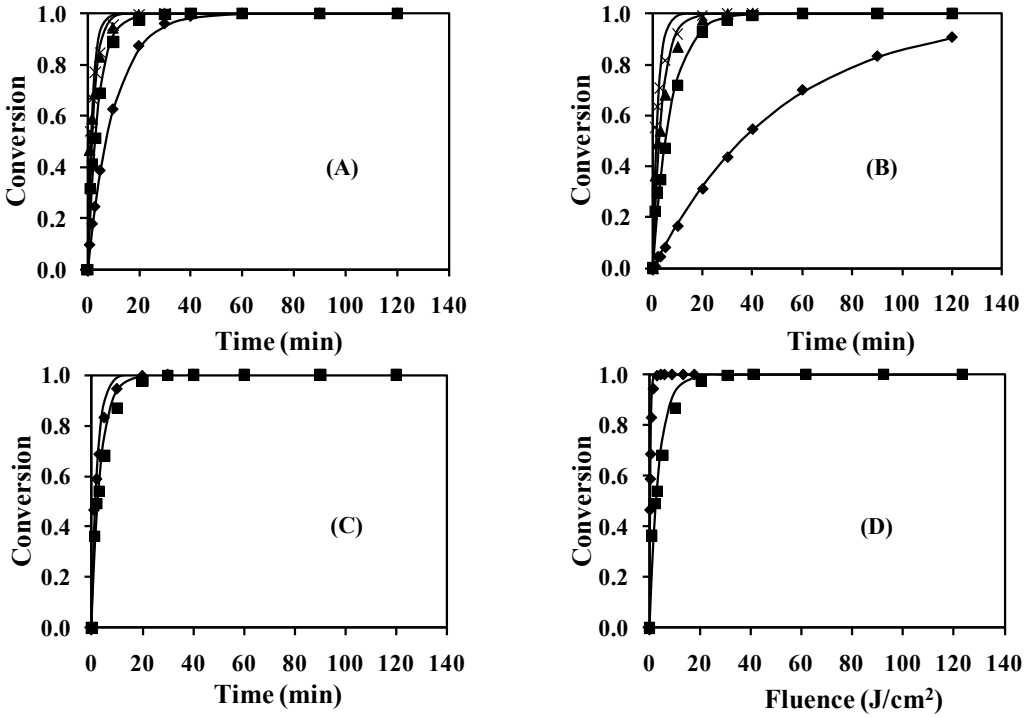

Figure 5. Variation of ferrous ions initial concentration: Amaranth conversion versus time, experimental and calculated values. **(A)**: KrCl excilamp. $[A]_0$ = 100 mg L^{-1}, V = 50 mL, mass ratio $[H_2O_2]_0$:$[A]_0$ = 5:1, $[Fe^{2+}]_0$ = ♦ 0, ■ 2.5, ▲5, x7.5 mg L^{-1} and (-) model. **(B)**: XeBr excilamp. $[A]_0$ = 100 mg L^{-1}, V = 50 ml, mass ratio $[H_2O_2]_0$:$[A]_0$ =6:1, $[Fe^{2+}]_0$ = ♦ 0, ■ 2.5, ▲ 5, x7.5 mg L^{-1} and (-) model. **(C)**: Amaranth conversion versus time, experimental and calculated values for the optimum $[Fe^{2+}]_0$ = 5 mg L^{-1}. Excilamp: ♦KrCl, ■ XeBr, (-) model.**(D)**: Amaranth conversion versus fluence with the optimum $[Fe^{2+}]_0$ = 5 mg L^{-1}. Excilamp: ♦KrCl, ■ XeBr, (-) model.

Figure 6

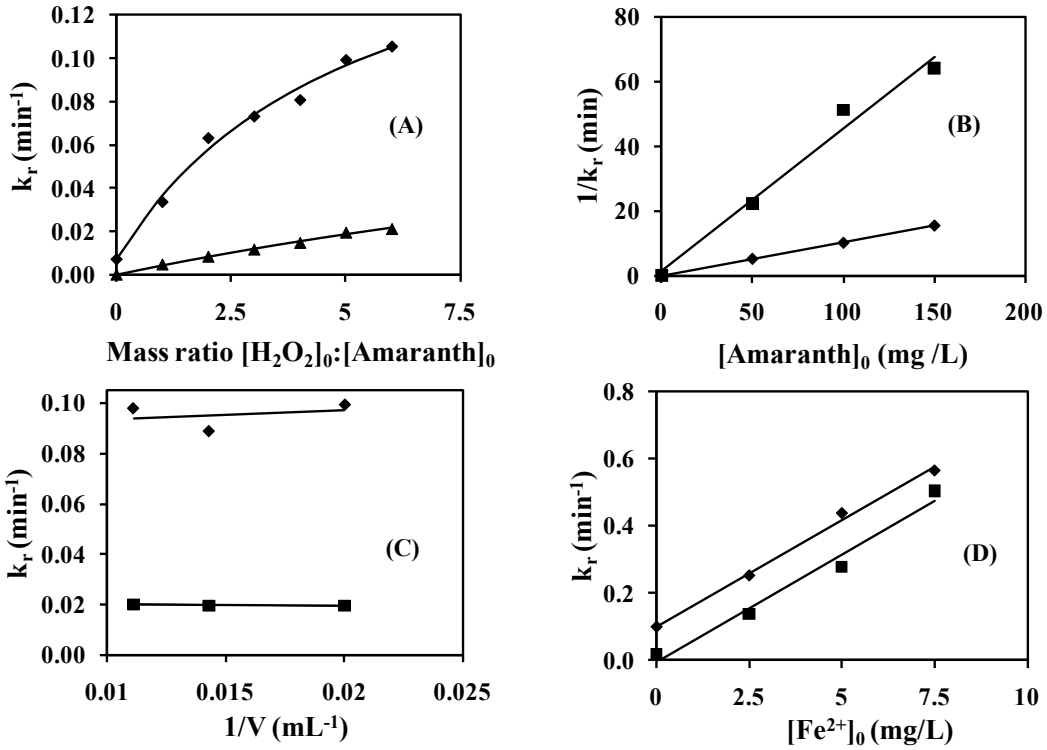

Figure 6. Influence of operational variables on the apparent kinetic constant for the batch reactor. (**A):** $[H_2O_2]_0$:$[A]_0$ mass ratio. **(B)**:Initial concentration of amaranth. **(C)**: Reaction volume. **(D)** Ferrous cation Fe^{2+}. Excilamp: ♦KrCl, ■ XeBr.

Figure 7

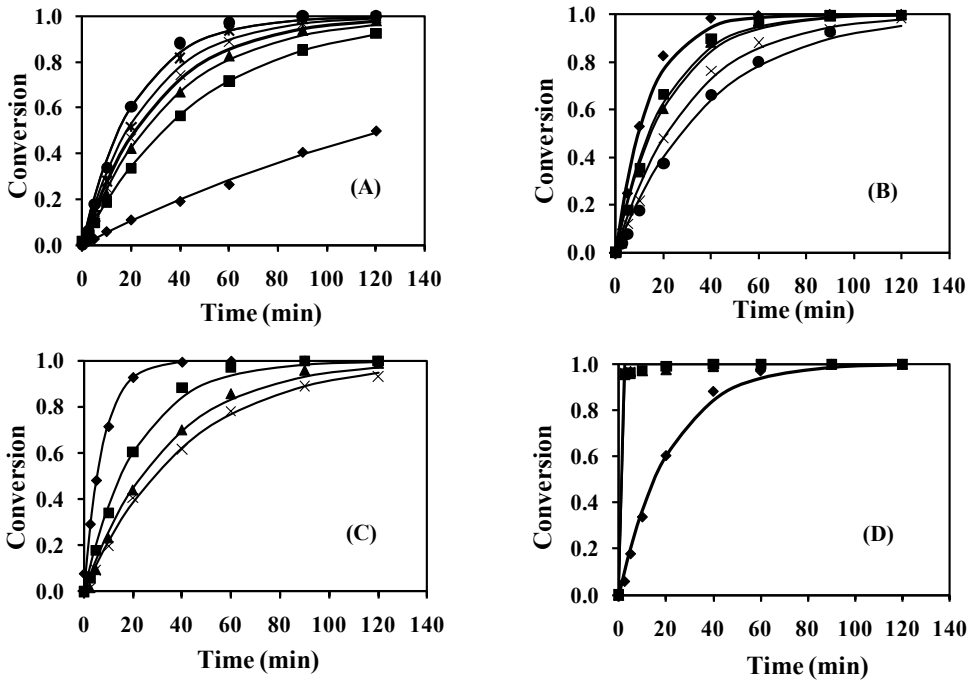

Figure 7. Amaranth conversion versus time, experimental and calculated values for the KrCl flow-through photoreactor. **(A)**: Variation of $[H_2O_2]_0$:$[A]_0$ mass ratio. $[A]_0$ = 100 mgL^{-1}, V = 250 mL, $[Fe^{2+}]_0$ = 0 mgL^{-1}, $[H_2O_2]_0$:$[A]_0$ mass ratio = ♦ 0:1, ■ 0.5:1, ▲1:1, x1.5:1, *2:1, ●2.5:1, + 3:1, (-) model. **(B)**:Variation of amaranth initial concentration. $[H_2O_2]_0$:$[A]_0$ mass ratio = 2.5:1, V = 250 mL, $[Fe^{2+}]_0$ = 0 mg L^{-1}, $[A]_0$ (mg L^{-1}) = ♦50, ■ 75, ▲100, x125, ●150, (-) model. **(C):** Variation of reaction volume. $[A]_0$ = 100 mg L^{-1}, $[H_2O_2]_0$:$[A]_0$ mass ratio = 2.5:1, $[Fe^{2+}]_0$ = 0 mg L^{-1}. V (mL) = ♦125, ■ 250, ▲375, x500 mL, (-) model. **(D)**: Variation of ferrous ions initial concentration. $[A]_0$ = 100 mg L^{-1}, $[H_2O_2]_0$:$[A]_0$ mass ratio =2.5:1, V = 250 mL, , $[Fe^{2+}]_0$ (mg L^{-1}) = ♦ 0.0, ■ 0.25, ▲ 0.5, x1.

Figure 8

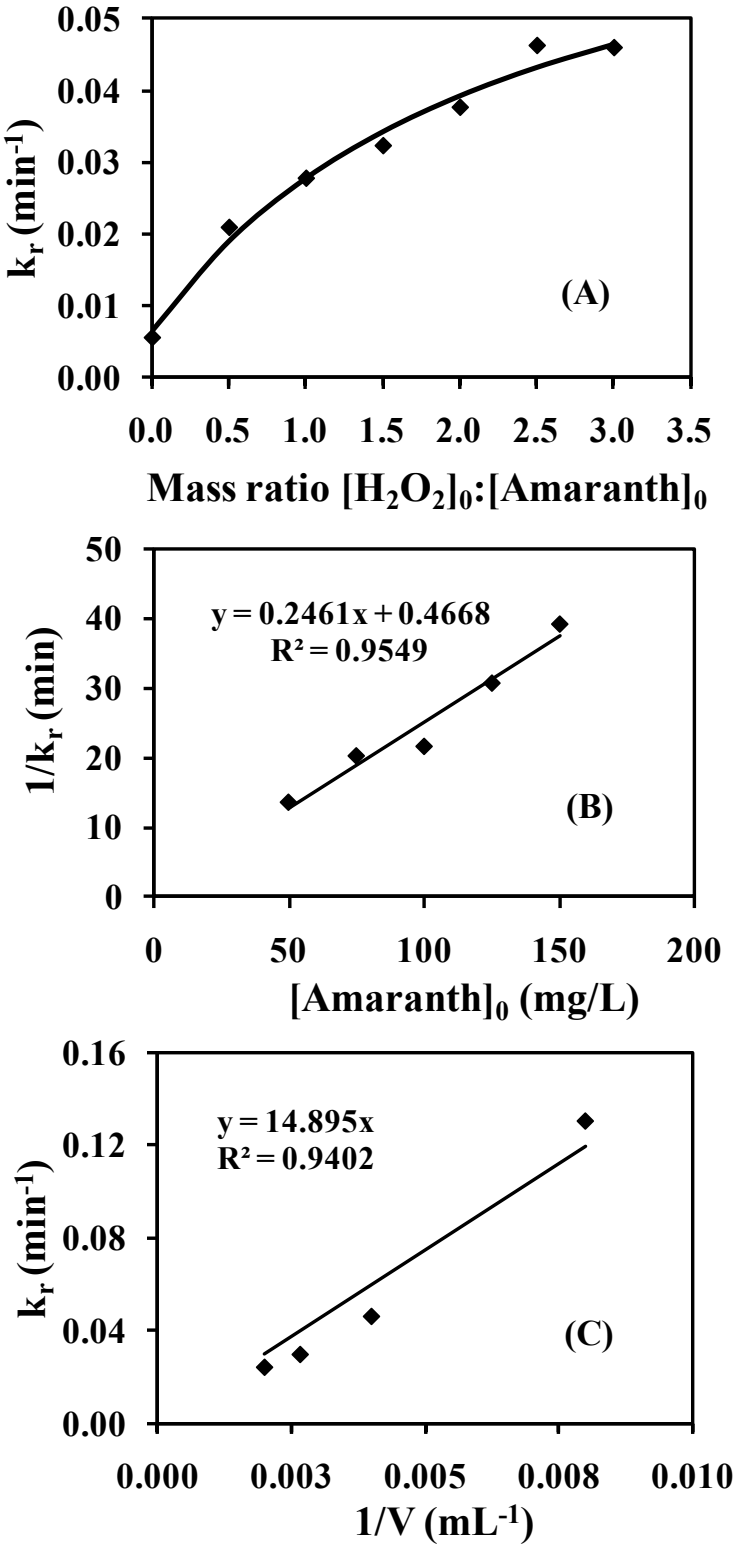

Figure 8. Influence of operational variables on the apparent kinetic constant for the KrCl flow-through photoreactor. (**A):**$[H_2O_2]_0$:$[A]_0$ mass ratio. **(B)**: Initial concentration of amaranth. **(C)**: Reaction volume.

Figure captions

Figure 1. Experimental reaction system, **(A)**: Static excilamp batch reactor and **(B)**:KrCl flow-through photoreactor.

Figure 2. Variation of $[H_2O_2]_0$:$[A]_0$ mass ratio; Amaranth conversion versus time, experimental and calculated values. **(A)**: KrCl excilamp. $[A]_0$ = 100 mg L^{-1}, V = 50 mL, $[Fe^{2+}]_0$ = 0 mg L^{-1}, $[H_2O_2]_0$:$[A]_0$ mass ratio = ♦ 0:1, ■1:1, ▲2:1, x 3:1, *4:1, ●5:1, + 6:1, (-) model. **(B)**: XeBr excilamp. $[A]_0$ = 100 mg/l, V = 50 mL, $[Fe^{2+}]_0$ = 0 mg L^{-1},mass ratio $[H_2O_2]_0$:$[A]_0$ = ♦ 0:1, ■1:1, ▲2:1, x 3:1, *4:1, ●5:1, + 6:1, - 7:1, (-) model. **(C)**: Amaranth conversion versus time for the optimum $[H_2O_2]_0$:$[A]_0$ mass ratio. Excilamp: ♦KrCl, ■ XeBr, (-) model. **(D)**: Amaranth conversion versus fluence for the optimum $[H_2O_2]_0$:$[A]_0$ mass ratio. Excilamp: ♦KrCl, ■ XeBr, (-) model.

Figure 3. Variation of amaranth initial concentration, **(A)**: Amaranth conversion versus time, experimental and calculated values. **(B)**: Amaranth conversion versus fluence. Mass ratio $[H_2O_2]_0$:$[A]_0$ = 5:1 for KrCl and 6:1 for XeBr, V = 50 mL, $[Fe^{2+}]_0$ = 0 mg L^{-1}. Variation of $[A]_0$ (mg L^{-1}) = ♦KrCl 50, ■ KrCl 100, ▲KrCl 150, xXeBr 50, *XeBr 100, ●XeBr 150, (-) model.

Figure 4. Variation of reaction volume **(A)**: Amaranth conversion versus time, experimental and calculated values. **(B)**: Amaranth conversion versus fluence. $[A]_0$ = 100 mg L^{-1}, mass ratio $[H_2O_2]_0$:$[A]_0$ = 5:1 for KrCl and 6:1 for XeBr, $[Fe^{2+}]_0$ = 0 mg L^{-1}. Variation of V (mL) = ♦KrCl 50, ■ KrCl 70, ▲KrCl 90, xXeBr 50, *XeBr 70, ●XeBr 90, (-) model.

Figure 5. Variation of ferrous ions initial concentration: Amaranth conversion versus time, experimental and calculated values. **(A)**: KrCl excilamp. $[A]_0$ = 100 mg L^{-1}, V = 50 mL, mass ratio $[H_2O_2]_0$:$[A]_0$ = 5:1, $[Fe^{2+}]_0$ = ♦ 0, ■ 2.5, ▲5, x7.5 mg L^{-1} and (-) model. **(B)**: XeBr excilamp. $[A]_0$ = 100 mg L^{-1}, V = 50 ml, mass ratio $[H_2O_2]_0$:$[A]_0$ =6:1, $[Fe^{2+}]_0$ = ♦ 0, ■ 2.5, ▲ 5, x7.5 mg L^{-1} and (-) model. **(C)**: Amaranth conversion versus time, experimental and calculated values for the optimum $[Fe^{2+}]_0$ = 5 mg L^{-1}. Excilamp: ♦KrCl, ■ XeBr, (-) model.**(D)**: Amaranth conversion versus fluence with the optimum $[Fe^{2+}]_0$ = 5 mg L^{-1}. Excilamp: ♦KrCl, ■ XeBr, (-) model.

Figure 6. Influence of operational variables on the apparent kinetic constant for the batch reactor. (**A):** $[H_2O_2]_0$:$[A]_0$ mass ratio. **(B)**:Initial concentration of amaranth. **(C)**: Reaction volume. **(D)** Ferrous cation Fe^{2+}. Excilamp: ♦KrCl, ■ XeBr.

Figure 7. Amaranth conversion versus time, experimental and calculated values for the KrCl flow-through photoreactor. **(A)**: Variation of $[H_2O_2]_0$:$[A]_0$ mass ratio. $[A]_0$ = 100 mgL^{-1}, V = 250 mL, $[Fe^{2+}]_0$ = 0 mgL^{-1}, $[H_2O_2]_0$:$[A]_0$ mass ratio = ♦ 0:1, ■ 0.5:1, ▲1:1, x1.5:1, *2:1, ●2.5:1, + 3:1, (-) model. **(B)**:Variation of amaranth initial concentration. $[H_2O_2]_0$:$[A]_0$ mass ratio = 2.5:1, V = 250 mL, $[Fe^{2+}]_0$ = 0 mg L^{-1}, $[A]_0$ (mg L^{-1}) = ♦50, ■ 75, ▲100, x125, ●150, (-) model. **(C):** Variation of reaction volume. $[A]_0$ = 100 mg L^{-1}, $[H_2O_2]_0$:$[A]_0$ mass ratio = 2.5:1, $[Fe^{2+}]_0$ = 0 mg L^{-1}. V (mL) = ♦125, ■ 250, ▲375, x500 mL, (-) model. **(D)**: Variation of ferrous ions initial concentration. $[A]_0$ = 100 mg L^{-1}, $[H_2O_2]_0$:$[A]_0$ mass ratio =2.5:1, V = 250 mL, , $[Fe^{2+}]_0$ (mg L^{-1}) = ♦ 0.0, ■ 0.25, ▲ 0.5, x1.

Figure 8. Influence of operational variables on the apparent kinetic constant for the KrCl flow-through photoreactor. (**A):**$[H_2O_2]_0$:$[A]_0$ mass ratio. **(B)**: Initial concentration of amaranth. **(C)**: Reaction volume..

Table 1. Experimental conditions for all series with static excilamps and values of pseudo first order kinetic constant, k_r

Mass ratio $[H_2O_2]$:[Amaranth]	$[Amaranth]_0$ (mg/L)	$[H_2O_2]_0$ (mg/L)	V (mL)	$[Fe^{2+}]_0$ (mg/L)	k_r (min^{-1})	r
Experiments with KrCl static excilamps						
0:1	100	0	50	0	0.0072	0.9978
1:1		100			0.0337	0.9989
2:1		200			0.0632	0.9994
3:1		300			0.0732	0.9999
4:1		400			0.0808	0.9996
5:1		500			0.0993	0.9998
6:1		600			0.1055	0.9998
5:1	50	250	50	0	0.1929	0.9996
	100	500			0.0994	0.9998
	150	750			0.0654	0.9996
5:1	100	500	50	0	0.0993	0.9998
			70		0.0890	0.9996
			90		0.0979	0.9997
5:1	100	500	50	0.0	0.0993	0.9998
				2.5	0.2525	0.9957
				5.0	0.4388	0.9907
				7.5	0.5661	0.9877
Experiments with XeBr static excilamps						
0:1	100	0	50	0	0.0002	0.7521
1:1		100			0.0047	0.9959
2:1		200			0.0083	0.9985
3:1		300			0.0116	0.9988
4:1		400			0.0148	0.9997
5:1		500			0.0160	0.9983
6:1		600			0.0195	0.9996
7:1		700			0.0212	0.9986
6:1	50	300	50	0	0.0449	0.9998
	100	600			0.0195	0.9996
	150	900			0.0156	0.9995
6:1	100	600	50	0	0.0195	0.9996
			70		0.0197	0.9998
			90		0.0201	0.9994
6:1	100	600	50	0.0	0.0195	0.9996
				2.5	0.1388	0.9955
				5.0	0.2774	0.9876
				7.5	0.5044	0.9762

Table 2. Experimental conditions for all series with KrCl flow-through photoreactor and values of pseudo first order kinetic constant, k_r.

Mass ratio $[H_2O_2]$:[Amaranth]	$[Amaranth]_0$ (mg/L)	$[H_2O_2]_0$ (mg/L)	V (mL)	$[Fe^{2+}]_0$ (mg/L)	k_r (min^{-1})	r
0:1	100	0	250	0	0.0056	0.9984
0.5:1		50			0.0209	0.9998
1.0:1		100			0.0277	0.9991
1.5:1		150			0.0323	0.9972
2.0:1		200			0.0376	0.9961
2.5:1		250			0.0462	0.9975
3.0:1		300			0.0459	0.9976
2.5:1	50	125.0	250	0	0.0734	0.9935
	75	187.5			0.0493	0.9959
	100	250.0			0.0462	0.9975
	125	312.5			0.0390	0.9995
	150	375.0			0.0255	0.9968
2.5:1	100	250	125	0	0.1306	0.9968
			250		0.0462	0.9975
			375		0.0298	0.9972
			500		0.0242	0.9983
2.5:1	100	250	250	0	4.62e-2	0.9975
				0.25	1.32e+11	0.9987
				0.50	1.26e+11	0.9985
				1.00	1.22e+11	0.9986

Table 3. Fitting of k_r to equation 4.2. Calculated parameters and correlation coefficients for batch reactors.

Parameter	KrCl excilamp	XeBr excilamp	Units
a	0.0592	0.0034	mg L^{-1} min^{-2}
b	0.3085	0.1562	mg L^{-1} min^{-2}
c	8.4720	35.3251	mg L^{-1} min^{-1}
d	1.6218	1.3544	mg L^{-1} min^{-1}
r	0.9948	0.9982	dimensionless

Table 4. Fitting of k_r to equation 4.2. Calculated parameters and correlation coefficients for KrCl flow-through photoreactor

Parameter	KrCl photoreactor	Units
a	2.6000	mg L^{-1} min^{-2}
b	0.1380	mg L^{-1} min^{-2}
c	0.0413	mg L^{-1} min^{-1}
d	1.7700	mg L^{-1} min^{-1}
r	0.9919	dimensionless

Table 5. Comparison between different UV lamps and reactor configurations.

Data of research	Lamp type	Reactor configuration	Intensity mW/cm^2	[Dye] mg/L	Process type	k_r min^{-1}	Half-life min	Fluence J/cm^2
This work	KrCl	Batch	2.47	50	UV/H_2O_2	0.1929	3.6	0.5
This work	KrCl	Flow-trough	2.38	50	UV/H_2O_2	0.0734	9.4	1.3
This work	XeBr	Batch	17.12	50	UV/H_2O_2	0.0449	15.4	15.9
This work	KrCl	Batch	2.47	150	UV/H_2O_2	0.0654	10.6	1.6
This work	KrCl	Flow-trough	2.38	150	UV/H_2O_2	0.0255	27.2	3.9
This work	XeBr	Batch	17.12	150	UV/H_2O_2	0.0156	44.4	45.6
Ref. [21]	Hg	Batch	8.75	200	$UV/H_2O_2/Fe^{2+}$	0.0360	19.3	10.1
Ref. [40]	Hg	Batch	----	20	UV/O_3	0.1036	6.7	----